Tunable Remote Pinning of Domain Walls in Magnetic Nanowires

L. O'Brien,* D. Petit, E. R. Lewis, and R. P. Cowburn

Thin Film Magnetism Group, Cavendish Laboratory, University of Cambridge,
JJ Thomson Avenue, Cambridge CB3 0HE, United Kingdom

D. E. Read, J. Sampaio, H. T. Zeng, and A.-V. Jausovec

Experimental Solid State Group, Department of Physics, Blackett Laboratory, Imperial College London,
Prince Consort Road, London SW7 2AZ, United Kingdom
(Received 12 November 2010; published 24 February 2011)

Domain wall (DW) pinning in ferromagnetic nanowires is in general a complex process. Distortions of the DW shape make quantitative agreement between modeling and experiment difficult. Here we demonstrate pinning using nanometer scale localized stray fields. This type of interaction gives well-characterized, tailorable potential landscapes that do not appreciably distort the DW. Our experimental results are in excellent quantitative agreement with an Arrhenius-Néel model of depinning—a result only possible when the modeled potential profile agrees fully with that experienced by the DW.

Domain wall (DW) motion in ferromagnetic planar nanowires has received much attention due to its wide range of applications in both studying fundamental physical phenomena [1–4] and in potential technological devices [5–8]. The role of DW pinning in nanowires is crucial for these investigations. Experiments to probe pinning typically trap the DW by geometrically shaping the conduit in which the DW propagates [9–13]. Attempts to quantitatively model the system often use a quasiparticle treatment of the DW (where the DW structure is not affected by the local environment). In general, however, using a geometrical trap intrinsically results in complex distortions of the DW shape, making the DW no longer independent of the potential profile. Experimental results and quantitative determination of the experienced pinning profile are therefore difficult to reconcile with modeling. Nondistorting potentials are extremely desirable in experiments testing fundamental models, such as DW resonance and spin torque investigations [14,15]. We have previously proposed that using magnetostatic stray fields, localized on the nanometer length scale, it may be possible to achieve well-defined, tailorable, noncontact DW traps which do not appreciably perturb the DW structure [16]. In this work we show this is indeed possible by demonstrating excellent quantitative agreement between the room temperature depinning field of DWs from experimentally fabricated devices and an Arrhenius-Néel model of thermally activated depinning—a result only possible when the modeled potential profile agrees fully with that experienced by the DW.

The magnetostatic interaction with a magnetic bead has been shown to be a mutual trap to a DW [17]. Additionally, the stray fields from nanowire ends or other DWs have been reported to greatly affect the switching behavior of ferromagnetic strips, wires, and rings [18–20]. For these interactions, it is convenient to consider the DW in terms of the magnetostatic charge density, defined as $\rho = -\mu_0 \nabla \cdot \mathbf{M}$, that arises from the diverging inwards [outwards] magnetization $\mathbf{M}$ of the head to head (HH) [tail to tail (TT)] DW. Figure 1 shows both $\mathbf{M}$ [1(a)] and
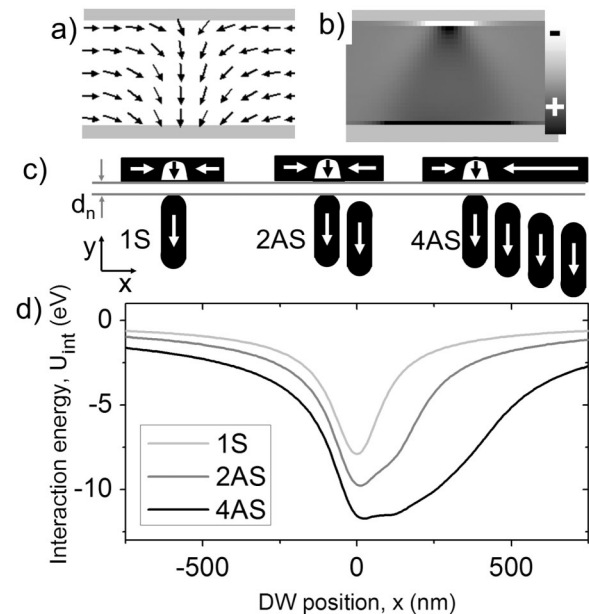

FIG. 1.   (a) Simulated micromagnetic configuration of a TDW in an 80 nm wide, 10 nm thick nanowire. (b) Corresponding magnetostatic charge distribution. White corresponds to a negative charge density, black to a positive charge density. (c) Schematics of the DW-trap configurations tested. A single stub gives a symmetric potential profile (1S), while the asymmetric two (2AS) and four (4AS) stubs traps give asymmetric profiles. (d) Plot showing potential landscape for the 1S (light gray), 2AS (dark gray), and 4AS (black) traps for $d_n = 40$ nm (see text for details).

ρ [1(b)] within a HH transverse DW (TDW), the lowest
energy DW configuration found in narrow, thin nanowires
[21–23]. The distributions are obtained using micromag-
netic simulations of a Permalloy (Py) nanowire with width
$w = 80$ nm, thickness $t = 10$ nm ($4 \times 4 \times 5$ nm^3 cell
size, $M_s = 800$ kA/m, $A = 13$ pJ/m, $\alpha = 0.5$) [24]. In
Fig. 1(b) black indicates positive magnetostatic charge
and white negative. It should be noted that the majority
of the TDW charge is located near the wide edge of the
DW [25]. It is the Coulomb-like interaction between this
DW charge distribution and that of additional locally gen-
erated charges that gives a potential landscape, $U_{int}(x)$.

For this Letter, the stray field arising from multiple
uniformly magnetized nanowire ends (hereafter termed
stubs) is used to demonstrate magnetostatic pinning of
the DW. First, numerical calculations of the potential
profiles for several of these magnetostatic DW traps are
presented, and the main features highlighted. A procedure
is then outlined for obtaining numerically the finite-
temperature magnetic field H_D required to overcome
pinning due to these potentials. Finally, we present experi-
mental measurements of H_D for such devices. As will be
seen, the good agreement between H_D indicates that the
modeled potential accurately reproduces the potential
experienced by the DW in the experimental system, and
that the DW structure is not appreciably perturbed in the
experiment.

The investigated geometries of a TDW interacting with
three different trap structures are schematically shown in
Fig. 1(c). The TDW passes the traps with its wide side
closest to the stub ends. The separation from the nearest
stub to the conduit is denoted d_n. Figure 1(d) shows the
numerically obtained U_{int} as a function of DW position for
the case when $d_n = 40$ nm. In these plots $t = 10$ nm. The
light gray profile shows U_{int} when the TDW passes a single
(76 nm wide) stub end of opposite charge (1S, symmetric
trap). The dark gray profile indicates U_{int} for a trap made
from two terraced (68 nm wide) stubs (2AS, asymmetric
trap), while the black profile is for four terraced (64 nm
wide) stubs (4AS, asymmetric trap). For both the 2AS and
4AS traps, the stubs are set at a pitch of 125 nm in x and
-20 nm in y. The geometries displayed are chosen to
match the experimentally tested devices, as described be-
low. In this work the potential U_{int} is calculated as in
Refs, [16,25]. All potential profiles are calculated using
the magnetostatic charge distribution of an isolated HH
TDW interacting with the charge distribution of isolated
stub ends. In considering only isolated charge distributions,
we assume that the interaction does not appreciably perturb
the DW structure. We may clearly see from Fig. 1(d) the
asymmetry the additional terraced stubs create. The wells
are extended in the $+x$ direction, reducing the potential
gradient on that side. Note, however, that the left-hand
side gradient and extent remain comparable. Thus, by
choosing the appropriate charge distribution it is possible

to artificially engineer the potential landscape experienced
by the DW.

The escape of a DW from the potential well formed by
the DW-stub interaction is a thermally activated process.
We model this as thermal activation over a single potential
barrier using an Arrhenius-Néel-type dependence:

$$\lambda(\delta\tau) = \frac{\delta\tau}{\tau_0} e^{-\Delta U_{int}/k_B T}. \tag{1}$$

Here $\lambda(\delta\tau)$ is the number of escape events in a time
interval $\delta\tau$, τ_0 is a characteristic attempt time, and ΔU_{int}
is the barrier height. For the case of a rigid DW, the
Zeeman energy due to an applied field, H, acts to shear
the potential landscape by $U_Z = -2\mu_0 M_S H w t x$, where x
is the DW position, w the conduit width, and t the conduit
thickness. This shear reduces the barrier height for DW
escape from a trap, increasing the probability of thermally
activated escape. At zero temperature, H_D is the field at
which the barrier height is 0 and is determined by the
steepest gradient of U_{int}. However, at finite-temperature
H_D corresponds to the field at which the barrier height is
reduced such that thermally activated escape occurs on the
characteristic time scale of the experiment. Crucially this
barrier height, ΔU_{int}, is highly dependent on both the initial
depth of the potential well and its complete shape. From
the numerical calculations outlined above, both U_{int} and
the effect of H upon barrier height are known, and thus a
value of the modeled room temperature H_D may be found.
In our experiments (see later) the sample rate, and there-
fore $\delta\tau$, is 1 ms. The field is approximately constant
over this time scale. Thus we examine the case where
$\delta\tau = 1$ ms and $\lambda(1$ ms$) = 1$ in Eq. (1). Estimates of τ_0
for micromagnetic switching processes vary over many
orders of magnitude from 10^{-7} to 10^{-12} s [26,27]. We
take $\tau_0 = 10^{-10}$ s [28], which gives a characteristic barrier
height the DW is able to overcome on a millisecond time
scale of $\Delta U_{int} \approx 16$ kT or 0.42 eV. Note that due to the
exponent, a change between $\tau_0 = 10^{-8}$ and 10^{-12} s cor-
responds to a change in ΔU_{int} of only a factor of 2 (from
0.29 to 0.51 eV), as would a similar ±2 orders of magni-
tude change in $\delta\tau$. As will be seen, this results in a change
of only ±3 Oe for the strongest interaction investigated.

To demonstrate magnetostatic pinning experimentally,
80 ± 4 nm wide, 10 ± 1 nm thick Py nanowires are pat-
terned into L shapes and act as a conduit for the DW. The
nanowires are produced using electron beam lithography
and thermal evaporation. The additional nanowire stub
traps are placed perpendicular to the long arm, as seen in
Fig. 2(b) for the case of a two stub trap (2AS). A global
magnetic field sequence, $H(t)$, is applied in the plane of the
device [see Fig. 2(b)]. Initially the structure is reset with a
saturating field in the $(-1, -1)$ direction, creating a HH
DW in the corner of the DW conduit. This field also sets
the magnetization of the stub traps in the $-y$ direction,
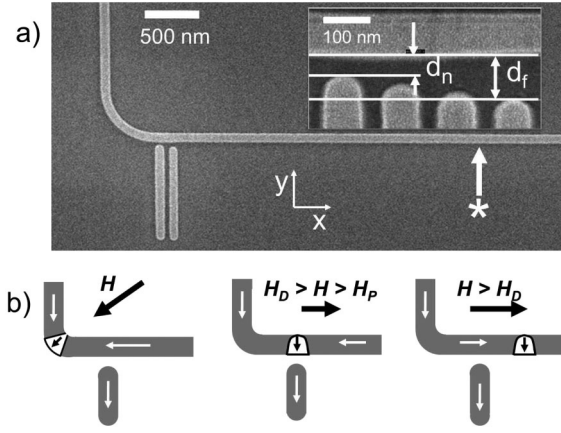creating negative charges along the edges near the conduit.

FIG. 2.   (a) SEM image of an experimental structure with a 2 stub trap (2AS). Switching of the nanowire at * indicates escape from the trap. Inset: Magnified image of interaction area between 4 stub trap (4AS) and DW. Indicated in the inset are the nearest stub separation d_n and final stub separation d_f. (b) Schematic of the magnetization evolution under applied global magnetic field sequence.

The magnitude of H is subsequently reduced to 0 Oe while its direction is maintained at $(-1, -1)$. The field is then increased in the $+x$ direction, at a rate of ~ 1 Oe/ms. When H exceeds the depinning field from the conduit corner, H_P (typically ~ 20 Oe for the 500 nm radius corner of our structures), the DW propagates along the conduit towards the localized pinning potential of the magnetostatic trap. To avoid transformations to the DW structure during propagation, the trap in each device is positioned in close proximity to the corner (~ 300 nm). This distance is significantly below the characteristic length scale over which transformations have been found to occur (the DW "fidelity" length, ~ 1.5 μm) [29]. The DW enters the local potential of the trap and remains pinned until the global magnetic field exceeds H_D. Once depinned, the DW continues to propagate along the conduit and switches the portion marked * in Fig. 2(a). Spatially resolved

magneto-optical Kerr effect measurements at position * are used to detect the switching of the DW conduit and therefore the field H_D at which the DW escapes from the trap. By varying d_n [i.e., the nearest stub separation; see inset Fig. 2(a)] over multiple structures, the dependence of H_D on both trap type and spacing is determined. Because of the geometry of the devices, only the right-hand edge of U_{int} may be probed. To measure both sides of the asymmetric potentials, reflected 4AS and 2AS traps are also used as indicated in the insets of Fig. 3. All distances are measured using scanning electron microscope (SEM) imaging. The average width $\hat{w} = 74 \pm 4$ nm for the 1S stub, $\hat{w} = 69 \pm 6$ nm for 2AS, and $\hat{w} = 65 \pm 5$ nm for 4AS. The pitch of the stubs is 125 nm in x and -20 nm in y for both the 2AS and 4AS devices.

Figures 3(a)–3(c) show the experimentally observed dependence of H_D on d_n for the 1S, 2AS, and 4AS traps, respectively. Each data point on the plots indicates an individual device. The gray squares in all plots indicate H_D when the last stub the DW passes is also the nearest to the conduit (see inset diagrams). In this case, for depinning to occur, the steeper side of the potential well, U_{int}, must be overcome (see Fig. 1). The black circles indicate structures where the shallower side must be overcome. In all plots we see a clear monotonic decrease in H_D as d_n increases, as would intuitively be expected. Figure 3(a) shows the simplest case when only a single stub traps the DW. The attractive interaction pins the DW up to ~ 94 Oe for $d_n = 23$ nm. For $d_n > 70$ nm the data are seen to plateau at $H_D \approx H_P \approx 20$ Oe, at which point pinning due to the corner becomes greater than pinning from the trap, and only H_P may be measured. The 4AS data of Fig. 3(c) show similar strong pinning for the steeper edge. The shallow edge pinning, however, displays a considerably weaker dependence on d_n with low values (~ 25 Oe) of H_D observed in all cases despite the close proximity of the trap. Similarly, in the two stub traps [2AS; Fig. 3(b)] the steeper edge pinning is found to be stronger than the shallower side, with a greater dependence on d_n observed.
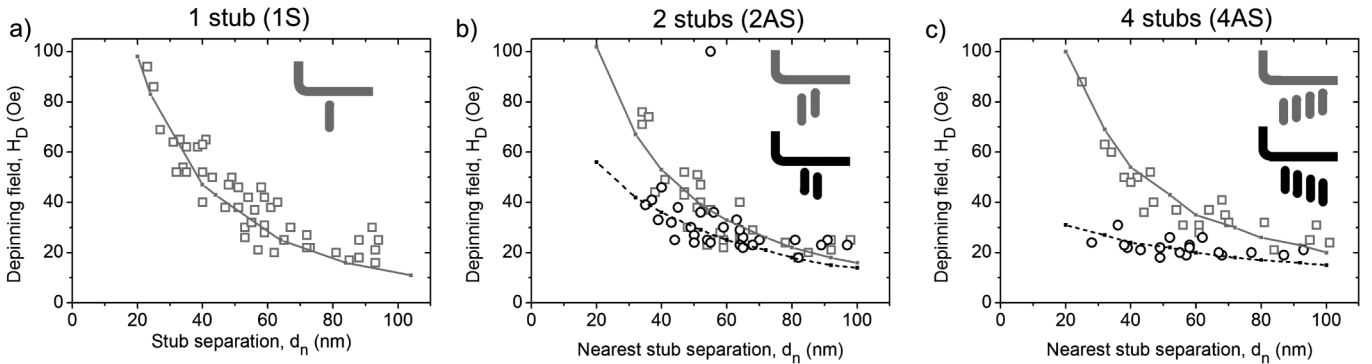

FIG. 3.   Experimentally obtained H_D as a function of nearest stub separation d_n. Steep side pinning is indicated by gray squares, shallow side by black circles. The gray solid and black dashed curves show H_D obtained for an Arrhenius-Néel thermally activated model using a magnetostatic charge-based description, with thickness $t = 10$ nm. Inset: Schematics of the trap geometry used: gray traps where the steeper edge is probed, black traps where the shallower edge is probed.

Now, however, the two data sets are comparable in magnitude and overlap is found between the two trends.

The line plots in Figs. 3(a)–3(c) indicate the modeled H_D values obtained from the calculations outlined earlier with $t = 10$ nm. The solid gray lines correspond to the stronger pinning from the steep well edge, and the dashed black lines from the weaker, shallower side. In general, we find an extremely close fit to the experimental data for all configurations and traps. The strong agreement suggests that the method implemented to describe the interaction is correct and that the TDW structure is indeed not appreciably perturbed for the dimensions tested, as has previously been suggested [12,16,30]. This is further supported by the results of micromagnetic simulations, where the TDW shape can indeed be seen to remain relatively unperturbed by the interaction (see supplemental material, Fig. 2 [31]). The agreement between the experimentally observed H_D and those found from modeling gives strong evidence that tailoring of the pinning potential is possible without modifying the TDW structure or wire shape. The effect of temperature on depinning also appears to agree with an Arrhenius-Néel-type activation over a single energy barrier. It should be noted that, for the strongest pinning values found (102 Oe, $2AS$ with $d_n = 20$ nm), using $\tau_0 = 10^{-8}$–10^{-12} s corresponds to a change of only ± 3 Oe in H_D. This relative insensitivity on the parameters $\delta\tau$ and τ_0 reduces the associated error from the unknown terms, but means robust conclusions on the semiphenomenological attempt frequency $1/\tau_0$ cannot be drawn. The clear asymmetry of H_D in asymmetric devices demonstrates that not only the initial depth (which would be independent of the side of the potential probed) but additionally the complete shape of a profile are essential in understanding the depinning of a DW, and highlights the strong agreement of the modeling with experiments. Finally, it might be argued that the pinning may be dominated simply by the final stub experienced by the DW, i.e., the rightmost in Fig. 2(a). If this were true, H_D would match that found for a single stub d_f from the conduit [the final stub separation; see inset Fig. 2(a)]. Fitting the data in this manner (see supplemental material, Fig. 1 [31]) shows this is not the case. It highlights the fact the resulting potential is a contribution from all of the individual pinning elements in the trap.

In conclusion, tailorable remote pinning of DWs has been demonstrated using magnetostatic interactions. This form of pinning offers well-characterized potential landscapes that do not appreciably perturb the DW structure. Experimentally obtained room temperature depinning field values agree completely with rigid, magnetostatic charge-based modeling using an Arrhenius-Néel-type

thermal activation over a single energy barrier. This result is only possible if the depth and complete shape of the modeled potential agree fully with that experienced by the DW.

*lao24@cam.ac.uk
[1] J. C. Slonczewski, J. Magn. Magn. Mater. **159**, L1 (1996).
[2] T. A. Moore *et al.*, Phys. Rev. B **80**, 132403 (2009).
[3] S. Ladak *et al.*, Nature Phys. **6**, 359 (2010).
[4] S. A. Yang *et al.*, Phys. Rev. Lett. **102**, 067201 (2009).
[5] S. S. P. Parkin, M. Hayashi, and L. Thomas, Science **320**, 190 (2008).
[6] D. A. Allwood *et al.*, Science **309**, 1688 (2005).
[7] A. Bisig *et al.*, Appl. Phys. Lett. **95**, 162504 (2009).
[8] D. A. Allwood *et al.*, Appl. Phys. Lett. **89**, 014102 (2006).
[9] R. D. McMichael *et al.*, J. Appl. Phys. **87**, 7058 (2000).
[10] J. Wunderlich *et al.*, IEEE Trans. Magn. **37**, 2104 (2001).
[11] A. Himeno *et al.*, J. Appl. Phys. **93**, 8430 (2003).
[12] D. Bedau *et al.*, Phys. Rev. Lett. **101**, 256602 (2008).
[13] M. Hayashi *et al.*, Appl. Phys. Lett. **92**, 162503 (2008).
[14] R. Moriya *et al.*, Nature Phys. **4**, 368 (2008).
[15] S. Lepadatu *et al.*, Phys. Rev. B **81**, 020413 (2010).
[16] L. O'Brien *et al.*, Phys. Rev. Lett. **103**, 077206 (2009).
[17] G. Vieira *et al.*, Phys. Rev. Lett. **103**, 128101 (2009).
[18] S. Goolaup, A. O. Adeyeye, and N. Singh, J. Appl. Phys. **100**, 114301 (2006).
[19] S. Basu *et al.*, J. Appl. Phys. **105**, 083901 (2009).
[20] M. Laufenberg *et al.*, Appl. Phys. Lett. **88**, 212510 (2006).
[21] R. D. McMichael and M. J. Donahue, IEEE Trans. Magn. **33**, 4167 (1997).
[22] M. Klaui *et al.*, Appl. Phys. Lett. **85**, 5637 (2004).
[23] Y. Nakatani, A. Thiaville, and J. Miltat, J. Magn. Magn. Mater. **290–291**, 750 (2005).
[24] M. J. Donahue and D. G. Porter, NIST Interagency Report No. NISTIR 6376, 1999.
[25] H. T. Zeng *et al.*, J. Magn. Magn. Mater. **322**, 2010 (2010).
[26] G. Bertotti, *Hysteresis in Magnetism* (Academic, San Diego, CA, 1998).
[27] T. A. Moore and J. A. C. Bland, J. Phys. Condens. Matter **16**, R1369 (2004).
[28] A. Himeno *et al.*, J. Magn. Magn. Mater. **286**, 167 (2005).
[29] E. R. Lewis *et al.*, Phys. Rev. Lett. **102**, 057209 (2009).
[30] E. Saitoh *et al.*, Nature (London) **432**, 203 (2004).
[31] See supplemental material at http://link.aps.org/supplemental/10.1103/PhysRevLett.106.087204 for (1) experimentally obtained H_d as a function of final stub separation d_f and (2) micromagnetic simulations of a TDW interacting with a single stub trap (1S).